Journal of Solid State Chemistry 187 (2012) 35–44

Contents lists available at SciVerse ScienceDirect

Journal of Solid State Chemistry

journal homepage: www.elsevier.com/locate/jssc

# Crystal structure and characterization of the novel $NH^+ \cdots N$ hydrogen bonded polar crystal $[NH_2(CH_2)_4NH][BF_4]$

M. Wojtaś [a,*], A. Gągor [b], O. Czupiński [a], W. Medycki [c], R. Jakubas [a]

[a] Faculty of Chemistry, University of Wroclaw, Joliot-Curie 14, 50-383 Wroclaw, Poland
[b] W. Trzebiatowski Institute of Low Temperature and Structure Research, Polish Academy of Science, PO Box 1410, 50-950 Wroclaw, Poland
[c] Institute of Molecular Physics, Polish Academy of Science, Smoluchowskiego 17, 60-179 Poznań, Poland

ARTICLE INFO

*Article history:*
Received 7 November 2011
Received in revised form
12 December 2011
Accepted 14 December 2011
Available online 23 December 2011

*Keywords:*
Hybrid material
Single-protonated piperazinium cation
NLO

ABSTRACT

Dielectric properties and phase transitions of the piperazinium tetrafluoroborate ($[NH_2(CH_2)_4NH][BF_4]$, abbreviated as PFB) crystal are related to the one-dimensional arrangement of the cations linked by the bistable $NH^+ \cdots N$ hydrogen bonds and molecular motions of the $[BF_4]^-$ units. The crystal structure of $[NH_2(CH_2)_4NH][BF_4]$ is monoclinic at room temperature with the polar space group *Pn*. The polar/acentric properties of the room temperature phase IV have been confirmed by the piezoelectric and pyroelectric measurements. DSC measurements show that the compound undergoes three first-order structural phase transitions: at 421/411 K (heating/cooling), at 386/372 K and at 364/349 K. $^1H$ and $^{19}F$ NMR measurements indicate the reorientational motions of $[BF_4]^-$ anions and piperazinium(+) cations as well as the proton motion in the hydrogen-bonded chains of piperazine along the [001] direction. Over the phase I the isotropic reorientational motions or even self-diffusion of the cations and anions are expected. The conductivity measurements in the vicinity of the II–I PT indicate a superionic phase over the phase I.



## 1. Introduction

Acentric materials with a macroscopic polar order possess variety of useful properties such as: a second order nonlinear optical activity (NLO), piezoelectricity, pyroelectricity or ferroelectricity. These materials are interesting from the point of view of new technologies e.g.: electro-optical devices, information storage, switchable NLO devices and light modulators [1–7]. Hybrid inorganic–organic are one of the most extensively studied crystalline families of hybrids which combine the specific properties of the inorganic frameworks (electronic and magnetic properties, mechanical and thermal stability) and the intriguing features of the organic molecules such as the flexibility and the ability to form weak interactions [8–10]. Inorganic–organic hybrid complexes, based on small heterocyclic cations (pyridinium, imidazolium) and tetrahedral anions like $[BF_4]^-$, $ClO_4^-$, $ReO_4^-$, $IO_4^-$ and $CrO_3F^-$, $[A^+][BX_4^-]$ type salts (where *A*—organic heteroaromatic ammonium cations) [11–15] have tendency to exhibit ferroelectric order at the room temperature phases. In spite of the structural similarities the origin of polar properties was found to be different for these materials.

The motion of the tetrahedral anions ($BX_4^-$) plays a crucial role in the generation of ferroelectricity in the imidazolium salts: $[C_3N_2H_5][ClO_4]$ [16] and $[C_3N_2H_5][BF_4]$ [17]. In the case of the pyridinium analogs the reorientational motion of the cations about its pseudo-hexagonal axis of the aromatic ring appears to be crucial in the ferroelectric phase-transition mechanism [11–15]. $[A^+][BX_4^-]$ type compounds with more complex cations (e.g. substituted pyridinium cations: amino- or cyanopyridinium) does not show the ferroelectric order. Nevertheless, we have recently synthesized and characterized simple (1:1) derivatives with 2,4,6-trimethylpyridinium cations (TMP): $[TMP][ClO_4]$ and $[TMP][BF_4]$ which appeared to be a strong nonlinear optical and pyroelectric materials at room temperature [18,19]. The polarity of these connections is due to the ferroelectric-type arrangements of the permanent electric dipoles of the methylpyridinium cations. On the other hand, the molecular mechanism of numerous phase transitions in these compounds is assigned to the dynamics of tetrafluoroborate groups. Since the role of dynamics of small cationic moieties in the generation of ferroelectricity in $[A^+][BX_4^-]$ type compounds is not well recognized we have extended our studies on the piperazinium analogs. Herein, we report a new interesting polar framework material based on the piperazine, $[NH_2(CH_2)_4NH][BF_4]$ (abbreviated as PFB) which displays complex sequence of the solid–solid phase transitions. In this paper the microscopic origin of the piezoelectricity and pyroelectricity and the mechanism of the phase transitions is

* Corresponding author.
*E-mail address:* maciej.wojtas@chem.uni.wroc.pl (M. Wojtaś).

0022-4596/$ - see front matter © 2011 Elsevier Inc. All rights reserved.
doi:10.1016/j.jssc.2011.12.020

discussed on the basis of the X-ray diffraction and NMR results. The thermal, dielectric and vibrational properties are also presented.

## 2. Experimental

The piperazine (99%, Sigma-Aldrich) was solubilized in concentrated $HBF_4$ (50%, Riedel-deHaën). The colourless, plate shaped crystals of $[NH_2(CH_2)_4NH][BF_4]$ were obtained by the slow evaporation of this solution.

DSC measurements on powdered samples were carried out using a Perkin Elmer DSC-7 in the temperature range 100–450 K with a scan rate of 10 K $min^{-1}$.

TGA and DTA were made on a Setaram SETSYS 16/18 instrument in a nitrogen atmosphere. The sample mass was 6.453 mg, the heating rate 2 K $min^{-1}$, and the temperature range 300–650 K. The complex electric permittivity, $\epsilon^* = \epsilon' - i\epsilon''$, was measured by a E4980A Precision LCR Meter within the frequency range from 500 Hz to 2 MHz and in the temperature range within 100–420 K. The dimensions of the sample were of the order of $5 \times 3 \times 1$ $mm^3$. The overall error for the real and imaginary parts of the complex electric permittivity was less than 5% and 10%, respectively.

The spontaneous polarization was measured by a charge integration technique using a Keithley 617 Programmable Electrometer. The temperature was stabilized by an Instec STC200 temperature controller.

The dilatometric measurements were accomplished by a thermomechanical analyzer Perkin Elmer TMA-7 within the temperature range 100–420 K. The dimensions of the sample were of the order of $11 \times 8 \times 4$ $mm^3$.

The NMR measurements were made using an ELLAB TEL-Atomic PS 15 spectrometer. Proton spin–lattice relaxation times $T_1$ at 25 MHz and fluorine $^{19}F$ spin–lattice relaxation times $T_1$ at 26.6 MHz were measured using an appropriate saturation sequence of $\pi/2$ pulses followed by a variable time interval $\tau$ and a reading $\pi/2$ pulse. The magnetization was found to recover exponentially within experimental error in following temperature regions: for proton between 102–344 K and above 421 K and for fluorine above 135 K up to 441 K. In the residual temperature regions the found non-exponentiality was well fitted using simple sum of two exponential functions. The temperature of the sample was controlled by a UNIPAN 650 temperature controller operating on Pt-100 sensor providing long time temperature stability better than 1 K. The sample of powdered $[NH_2(CH_2)_4NH][BF_4]$ was evacuated at room temperature and then sealed under vacuum in a glass ampoule. All measurements were made on heating the sample from liquid nitrogen temperature. The errors in the measurements of $T_1$ were estimated to be about 5%.

Temperature dependent infrared spectra were recorded with the resolution of 1 $cm^{-1}$ in the range 4000–400 $cm^{-1}$ using a Nicolet Avatar FT-IR spectrometer. The samples were prepared as suspensions of powder crystal in Nujol medium and measured between KBr windows in the temperature range 300–408 K. A variable-temperature Graseby–Specac cell was used to control the temperature. The stability of the temperature was $\pm 1$ K. For the spectroscopic data analysis the multifunctional Galactic GRAMS/386 program was used.

Raman spectra of a powdered crystal at room temperature were recorded using a Nicolet Magna 860 FT-IR spectrometer, interfaced with a FT-Raman accessory ($CaF_2$ beamsplitter and InGaAs detector). The Raman spectra were excited with a Nd:$YVO_4$ laser line at 1064 nm with a power of ca. 290 mW. The measurements were performed over the wavenumber range 3700–100 $cm^{-1}$ with resolution of 4 $cm^{-1}$.

Single crystal X-ray diffraction data were collected using four circle diffractometer operating in κ-geometry. The CrysAlis. software version 1.170.32 [20] was used for data processing. Empirical absorption correction was done using spherical harmonics, implemented in SCALE3 ABSPACK scaling algorithm. The structure was solved by direct methods and refined by means of SHELX-97 program package [21]. The H atoms in $CH_2$ groups were included in geometric positions and treated as a riding atoms. The positions of hydrogen atoms from $NH_2^+$ and NH groups were taken from difference Fourier maps and were refined with the distance restraints. The $U_{iso}(H)$ were constrained to be $xU_{eq}$(carrier atom), where $x = 1.2$. High temperature was maintained in a simple high-temperature attachment with hot-air flow (Kuma Diffraction, covering the temperature range 300–770 K). The crystal structure at room temperature was solved in non-centrosymmetric *Pn* space group. Although the symmetry tests basing on the atoms positions suggest the centrosymmetric $P2_1/n$ symmetry the results of piezoelectric effect measurements confirm the lack of the inversion centre in the crystal structure. $[NH_2(CH_2)_4NH][BF_4]$ is a weak scatterer, mainly due to the presence of the light atoms in the crystal structure and pronounced disorder of the $[BF_4]^-$ groups. Also a low mosaicity induced by the fast growth of the crystals affects the diffraction intensities. Thus, the data to parameter ratio is low. The compound is also a weak anomalous scatterer. The crystal data, data collection and refinement details are presented in Table 1. CCDC 842195 contains the crystal information data file for the structure.

$[NH_2(CH_2)_4NH][BF_4]$ exhibits several phase transitions at high temperatures. Due to the huge lattice distortion that accompanies IV to III PT and leads to the sample cracking and decay of the diffracted intensities only the crystal structure of the IV, room temperature phase was solved from single-crystal X-ray diffraction.

Powder diffraction data were collected at X'Pert PRO X-ray Diffraction system equipped with PIXcel ultra-fast line detector, focusing mirror and Soller slits for Cu $K\alpha$ radiation. The samples

**Table 1**
Crystal data, data collection and refinement results for $[NH_2(CH_2)_4NH][BF_4]$.

| | |
|---|---|
| **Crystal data** | |
| Chemical formula | $C_4H_{11}BF_4N_2$ |
| $M_r$ | 173.96 |
| Crystal system, space group | Monoclinic, *Pn* |
| Temperature (K) | 295 |
| *a*,*b*,*c* (Å) | 8.432 (1), 9.176 (1), 9.565 (1) |
| $\beta$ (°) | 98.42 (1) |
| $V$ (Å$^3$) | 732.2 (2) |
| $Z$ | 4 |
| Radiation type | Mo K $\alpha$ |
| $\mu$ ($mm^{-1}$) | 0.17 |
| Crystal size (mm) | 0.30 × 0.25 × 0.23 |
| **Data collection** | |
| Diffractometer | KM4-CCD |
| Absorption correction | Multi-scan. |
| Tmin, Tmax | 0.95, 0.96 |
| No. of measured, independent and observed $[I > 2\sigma(I)]$ reflections | 7410, 2603, 1524 |
| $R_{int}$ | 0.05 |
| **Refinement** | |
| $R[F^2 > 2\sigma(F2)]$, $wR(F^2)$, $S$ | 0.051, 0.136, 0.9 |
| No. of reflections | 2603 |
| No. of parameters | 216 |
| No. of restraints | 7 |
| $\Delta\rho_{max}$, $\Delta\rho_{min}$ (e Å$^{-3}$) | 0.33, −0.21 |

were measured in Bragg–Brentano geometry in the Anton Paar 1200N High-Temperature Oven Chamber.

## 3. Thermal behaviour

The differential scanning calorimetry (DSC) cooling and heating runs are presented in Fig. 1. Part (a), entitled "scan 1" shows the first runs of the virgin, not powdered sample on heating up to the phase II and cooling down to phase IV. Part (b), i.e. "scan 2" shows the runs on heating and cooling in the temperature scope ranging all the phases from IV to I. It is clearly seen that reaching the highest temperature phase does not affect the reproducibility (i.e. reversibility and enthalpies) of all the phase transitions. We carried out also the same DSC experiments but on well comminuted sample. It appeared that the level of fragmentation of the crystal slightly affects the phase transition temperatures of $[NH_2(CH_2)_4NH][BF_4]$ (the PTs temperatures are shifted by about 5° comparing to crystalline sample) but has no influence on their reproducibility.

All the phase transitions are manifested as peaks what indicates that the crystal undergoes three phase transitions of the discontinuous type. The I↔II phase transition (PT) is characterized by the entropy, $\Delta S_{tr}$, that equals to 11.2, what is c.a. $R\ln 4$. The entropy of the II↔III and III↔IV PTs amounts to 6.5 and 7.6 ($\approx R\ln 2$ in both cases), respectively. These values of $\Delta S_{tr}$ indicate that all the phase transitions are related to the big changes in dynamical situation of the cations and the anions.

Results of the thermogravimetric analysis are presented in Fig. 2. $[NH_2(CH_2)_4NH][BF_4]$ seems to be stable up to about 350 K when continuant decomposition starts down to c.a. 2% of initial mass of the sample. It must be noted, however that at about 385 K and 420 K (i.e. temperature of the III→II and II→I phase transitions, respectively) the weight of the sample diminishes jumpwisely (see inset in Fig. 2). This might be related both to the thermal desorption of contaminants of sample's surface (dominating in phase II, weight loss about 0.5%) and slow, initial decomposition of the crystal. At 370 K, 385 K and 420 K three endotherms are observed which are assigned to IV→III, III→II and II→I PTs, respectively. These PTs also are well separated in the DSC run on heating.

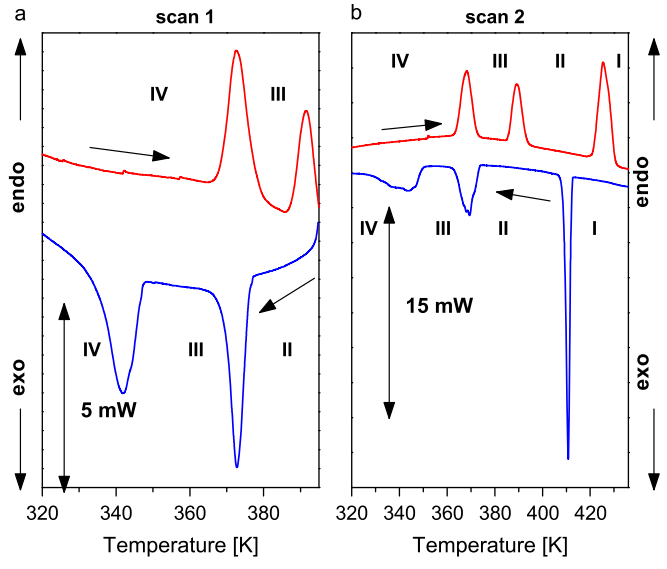


**Fig. 1.** DSC curves for $[NH_2(CH_2)_4NH][BF_4]$.

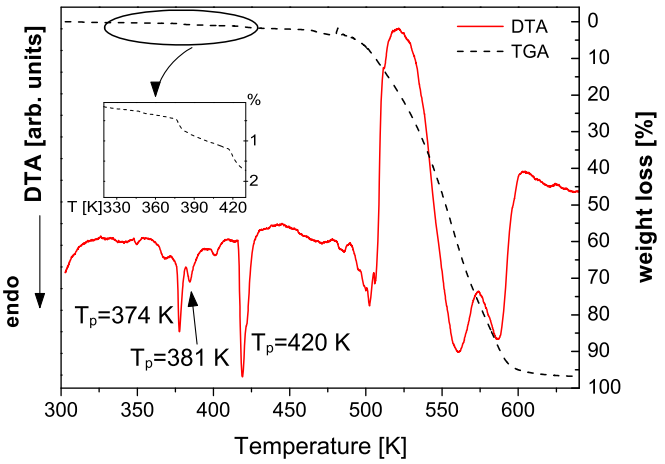


**Fig. 2.** Simultaneous thermogravimetric analysis (TGA) and differential thermal analysis (DTA) scans for $[NH_2(CH_2)_4NH][BF_4]$. The scans were performed in flowing nitrogen with a ramp rate of 5 K min$^{-1}$ (selected single crystals, atmosphere: nitrogen, flow rate 1 dm$^3$ h$^{-1}$). Inset shows the weight loss in the vicinity of the II→I PT.

Dilatometric measurements results are presented in Fig. 13 in the Supplementary Materials.

It is worth of note that the phase transitions observed by means of DSC, TGA and dilatometric technique are in good agreement to each other. Basing on the results presented above one may construct the following diagram of phase transitions:

Phase IV $\underset{349}{\overset{364}{\rightleftharpoons}}$ phase III (discontinuous, $\Delta S_{tr} = 7.6$ J/mol K $\approx R\ln 2$)

Phase III $\underset{372}{\overset{386}{\rightleftharpoons}}$ phase II (discontinuous, $\Delta S_{tr} = 6.5$ J/mol K $\approx R\ln 2$), whitening of the crystal

Phase II $\underset{411}{\overset{421}{\rightleftharpoons}}$ phase I (discontinuous, $\Delta S_{tr} = 11.2$ J/mol K $\approx R\ln 4$).

## 4. X-ray measurements

### 4.1. Crystal structure at room temperature, phase IV

Piperazinium tetrafluoroborate is a rare example of the inorganic salt with the single protonated piperazinium cation. Most of the piperazinium salts contain doubly protonated counterions, a concise results of the CCDC database survey are presented in [22]. The singly protonated piperazinium ring possesses the chair conformation. The protonation does not have a significant impact on the ring geometry although the C–N distances to $NH_2^+$ group are slightly longer then C–NH bonds, see Table 4 in Supplementary materials.

The most important effect of the single protonation is the active NH acceptor center that allows neighbouring cations interact via strong N−H···N hydrogen bonds that control the spatial organization of the cation substructure. The hydrogen-bonded chains of piperazinium(+) expand along [001] direction. The $[BF_4]^-$ groups form stacks amongst the chains. Fig. 3 shows the crystal packing and hydrogen bonded chains of the piperazinium(+) cations. Asymmetric unit contains two independent piperazinium(+) cations (*A* and *B*) and two $[BF_4]^-$ anions showing pronounced thermal motion at room temperature. All atoms adopts $C_1$ symmetry sites thus the boron coordination is distorted tetrahedron. Both piperazinium(+) cations form numerous N−H···F bonds to $[BF_4]^-$ group. Particularly piperazinium B is a donor of hydrogen in five hydrogen bonds, see Table 2. Additionally carbon from the $CH_2$ groups serves as a donor in weak C−H···F bonds. All these interactions give three dimensional complex structure of hydrogen bonds at room temperature.

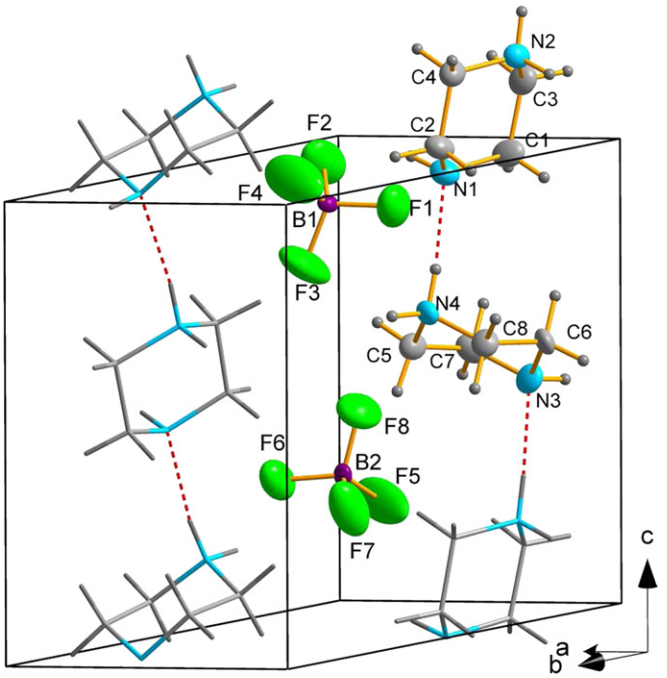


**Fig. 3.** The crystal packing of $[NH_2(CH_2)_4NH][BF_4]$, phase IV. The dashed lines stand for the hydrogen bonds. The hydrogen bonds to $[BF_4]^-$ groups are not included for the picture quality. Displacement parameters are drawn with 50% probability.

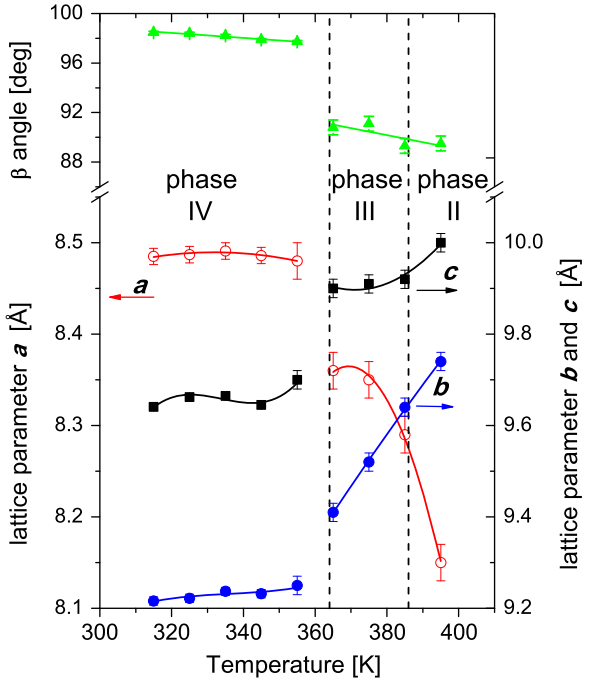


**Fig. 4.** Temperature evolution of lattice parameters in $[NH_2(CH_2)_4NH][BF_4]$. The lines are the guides for the eyes.

**Table 2**
Selected hydrogen-bond parameters at 295 K.

| D–H···A | D–H (Å) | H···A(Å) | D···A(Å) | D–H···A(°) |
|---|---|---|---|---|
| N2–H2A···N3[a] | 0.93(3) | 1.95(3) | 2.872(4) | 173(3) |
| N2–H2B···F2[b] | 0.97(1) | 2.21(2) | 3.011(4) | 139(2) |
| N2–H2B···F6[c] | 0.97(1) | 2.24(2) | 3.048(4) | 123(2) |
| N3–H3···F1[d] | 0.97(1) | 2.33(2) | 3.082(4) | 134(3) |
| N3–H3···F5[e] | 0.96(1) | 2.50(2) | 3.256(4) | 135(2) |
| N4–H4C···N1 | 0.99(2) | 1.93(2) | 2.865(4) | 160(3) |
| N4–H4D···F6 | 0.96(1) | 2.05(1) | 2.984(4) | 163(3) |
| N4–H4D···F7 | 0.96(1) | 2.34(2) | 3.086(4) | 135(2) |
| C7–H7A···F8[f] | 0.97 | 2.52 | 3.278(5) | 135 |
| C1–H1B···F[b] | 0.97 | 2.50 | 3.259(5) | 135 |
| C4–H4A···F7[g] | 0.97 | 2.43 | 3.285(5) | 146 |
| C6–H6B···F8[h] | 0.97 | 2.52 | 3.412(5) | 153 |
| C8–H8B···F3 | 0.97 | 2.37 | 3.199(5) | 143 |

[a] $x,y,z+1$.
[b] $x-1,y,z$.
[c] $x-1/2,-y+1,z+1/2$.
[d] $x-1/2,-y,z-1/2$.
[e] $x,y-1,z$.
[f] $x+1/2,-y+1,z-1/2$.
[g] $x+1/2,-y+1,z+1/2$.
[h] $x-1/2,-y+1,z-1/2$.

Two main contributions to the spontaneous polarization in the crystal structure of phase IV are expected. The main one comes from the internal dipole moment (DM) of piperaiznium cation, the second one is associated with the direction of hydrogen bonds. Single protonated piperazinium cation exhibit internal DM directed from NH to $NH_2^+$ group. In the phase IV all piperazinium chains are set in the same directions giving the summary DM in (a,c) plane as it is expected from *Pn* symmetry. All contributions in [010] direction are cancelled out. The dipoles associated with hydrogen bonds are set in opposite directions to the piperazinium dipoles diminishing the resultant bulk DM. Either internal DM of piperazinium(+) and DM of hydrogen bonds are determined by the position of $NH_2^+$ group. Thus, the proton transfer within the N–H···N bonds have a great impact on the dielectric properties of the crystal changing both the direction of the internal DM of piperazinium(+) and the direction of the dipole associated with the hydrogen bond.

### 4.2. Crystal structure and phase transitions at high temperatures

A huge distortion of the crystal structure accompanies the IV–III phase transition at 350 K. All lattice parameters change abruptly. Crystal elongates in the *b* and *c* direction with $\Delta b/b$ and $\Delta c/c$ c.a. 1.6%, and contracts in a direction with $\Delta a/a$ equal to 1.4% (see Fig. 4). The most pronounced change concerns however, the monoclinic $\beta$ angle that drop from 98° to 91°, which gives almost 7% $\Delta\beta/\beta$ decrease.

The metric of the crystal change after the transition. Powder X-ray diffraction gives numerous indexing possibilities for the high temperature phases although none of them could be confirmed by the structure solution. Fig. 5 presents the thermal evolution of diffraction intensities recorded for $[NH_2(CH_2)_4NH][BF_4]$. X-ray diffraction confirms complex phase situation at high temperatures. Four different structural phases are present. Since $[BF_4]^-$ groups in phase IV show pronounced thermal motion it seems that consecutive phase transitions arise as a result of competition between thermally activated disorder of $[BF_4]^-$ groups and stabilizing N–H···F interactions. It is also possible that at higher temperatures the N–H···N hydrogen bonds between piperazinium(+) cations are broken.

## 5. Dielectric studies

Temperature dependence of the real part of the complex electric permittivity, $\epsilon'$, along the $[20\bar{1}]$ direction at selected frequencies is displayed in Fig. 6. In the first heating cycle the $[NH_2(CH_2)_4NH][BF_4]$ compound clearly undergoes three first-order phase transitions (PTs). Two of them, at 364 and 421 K, are

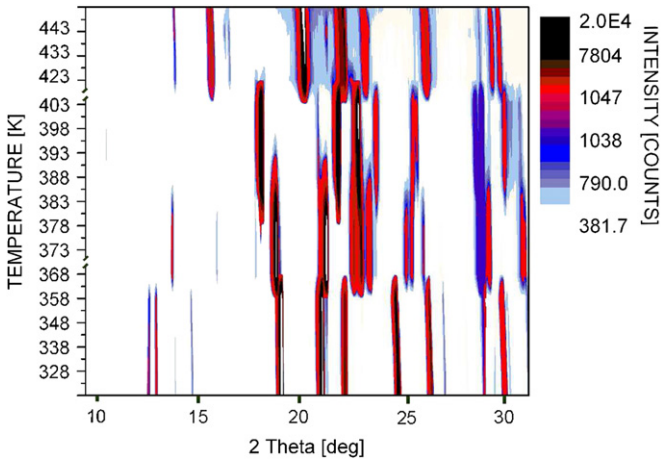


**Fig. 5.** Thermal evolution of diffraction intensities in $[NH_2(CH_2)_4NH][BF_4]$. Four different phases are present.

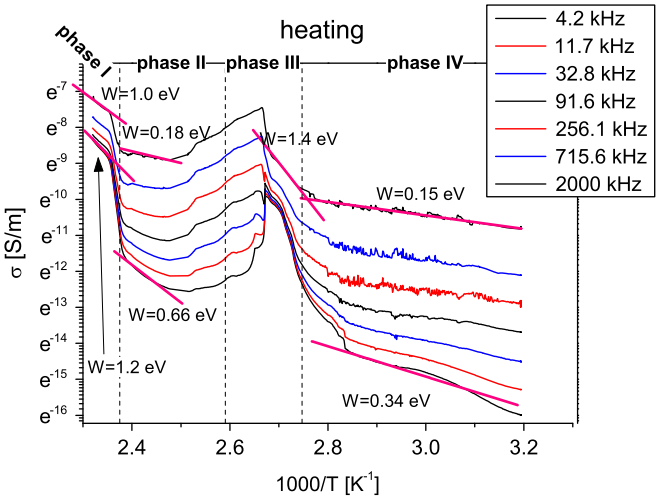


**Fig. 7.** Conductivity, $\sigma$, versus reciprocal temperature, $1000/T$, of $[NH_2(CH_2)_4NH][BF_4]$ measured in the $[20\bar{1}]$ direction.

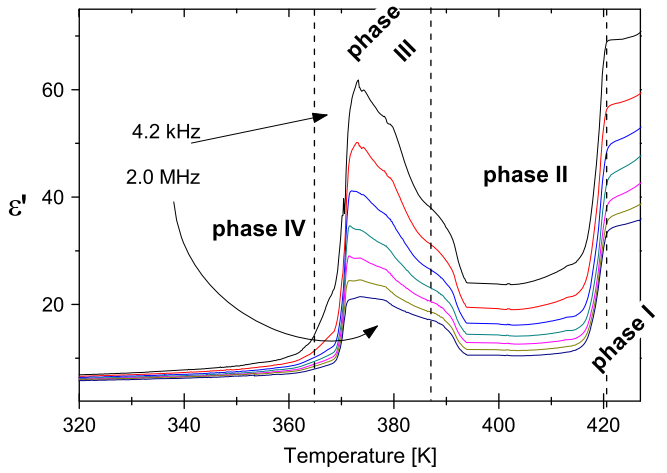


**Fig. 6.** $\epsilon'$ versus temperature on heating of $[NH_2(CH_2)_4NH][BF_4]$ measured in the $[20\bar{1}]$ direction.

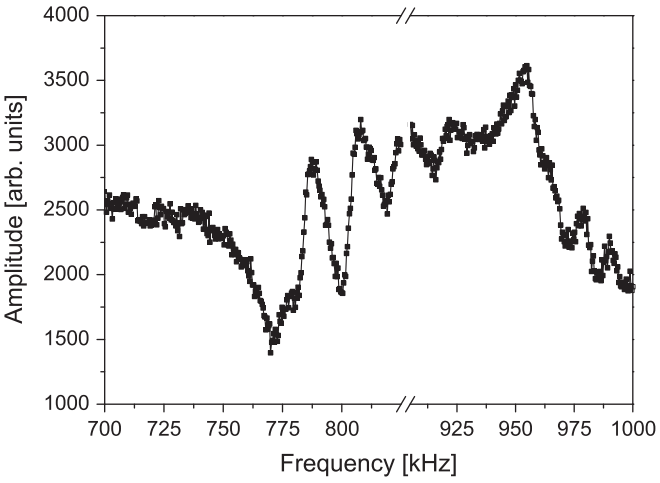


**Fig. 8.** The piezoelectric response of $[NH_2(CH_2)_4NH][BF_4]$ measured in the $[20\bar{1}]$ direction at ambient temperature.

manifested by step-like anomalies whereas the intermediate PT is smeared and takes place at ca. 386 K. The increase in $\epsilon'(T)$ is especially high at the (IV→III) and (II→I) PT with the dielectric increment of the order of 50–60. The dielectric response for the former transition resembles those ones encountered in ferroelectric materials and it really takes place between two polar phases (IV and III). On the other hand the PT from phase II to I is characteristic for crystals characterized by highly disordered high temperature phases (e.g. plastic/rotator phases). Since the dielectric dispersion process between 4 kHz and 2 MHz in the temperature range covering all phases was not observed we can conclude that the dipolar group motions are fast and are expected to be active in the microwave frequency region. The discrepancies of the permittivity approaching 421 K may be explained in terms of the electric conductivity arising at high temperatures.

In Fig. 7 the temperature dependence of the ac conductivity measured along the $[20\bar{1}]$ direction in the heating cycle above RT is presented. In the $\sigma(T)$ response two clear anomalies near 364 and 421 K are visible. The large conductivity above 421 K ($\sigma \approx 10^{-5}$ S/cm) corroborates the presence of the superionic phase. The activation energy along the $[20\bar{1}]$ direction in phase I is estimated to be about 1–1.2 eV while in ordered phase IV c.a. 0.15–0.34 eV.

## 6. Piezoelectric effect studies

The measurements of the piezoelectricity of $[NH_2(CH_2)_4NH][BF_4]$ were carried out only at room temperature in order to confirm the lack of the inversion center in the phase IV suggested by the X-ray diffraction. The studies were performed on the monocrystal sample in the $[20\bar{1}]$ direction. Since this direction is skewed to the main crystallographic axes of $[NH_2(CH_2)_4NH][BF_4]$ and the crystal symmetry is low we can treat the results only qualitatively. They are presented in Fig. 8. One can observe several piezoelectric resonances in the frequencies range of 775–825 kHz and 900–1000 kHz. This confirms unambiguously the lack of the inversion center at room temperature.

## 7. Pyroelectric effect studies

The results of the pyroelectric measurements are presented in Fig. 9. The sample of $[NH_2(CH_2)_4NH][BF_4]$ prepared for these measurements was oriented in the $[20\bar{1}]$ direction. The change of the spontaneous polarization, $\Delta P_s$, is of the order of $1 \times 10^{-8}$ C/m$^2$ what indicates that $[NH_2(CH_2)_4NH][BF_4]$ is a weak pyroelectric material. Moreover, according to the X-ray diffraction studies, the polarization vector lies in the *ac* plane and most

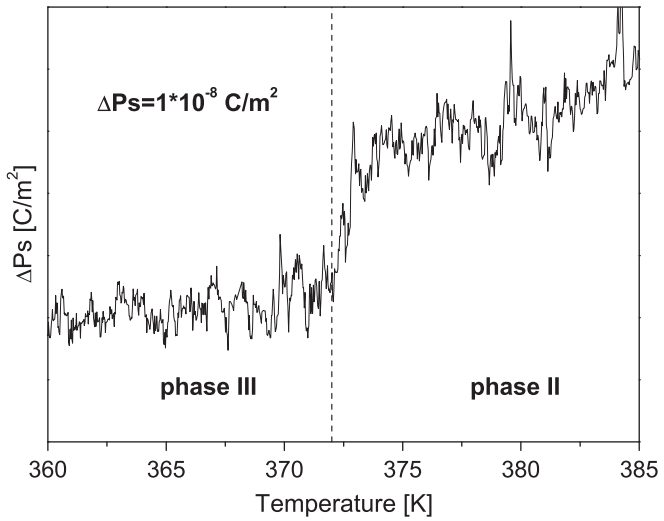


**Fig. 9.** The relative change of the spontaneous polarization, $\Delta P_s$, in the vicinity of the II→III phase transition of $[NH_2(CH_2)_4NH][BF_4]$ recorded on cooling in the $[20\bar{1}]$ direction.

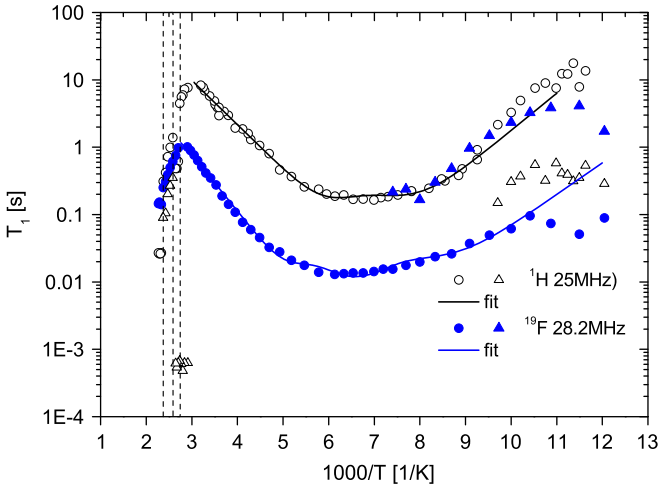


**Fig. 10.** Spin–lattice relaxation time, $T_1$, versus reciprocal temperature.

probably measured direction $[20\bar{1}]$ is not parallel to the polarization vector. Despite this the $\Delta P_s$ is clearly bigger than the level of noises.

## 8. NMR measurements

The experimental spin–lattice relaxation $T_1$ of proton $^1$H and fluorine nuclei $^{19}$F (violet and green dots, respectively) as a function of inverse of temperature ($1000/T$ [$K^{-1}$]) measured at 25 MHz and 26.6 MHz, respectively, are plotted in Fig. 10. It must be noted that the spin–lattice relaxation time of proton $^1$H as well as fluorine nuclei $^{19}$F has two components in certain temperature ranges.

The dependence of the long-component of spin–lattice relaxation $T_1$ time shows wide, slightly asymmetric minimum which comprises of two local minima of almost equal depth of about 190 and 240 ms at c.a. 123 K and 169 K, respectively. At higher temperatures, at about 316 K, the proton $T_1$ relaxation time reaches a maximum which is followed by its abrupt decrease. Such a temperature behavior of the $T_1$ may be explained by the changes in the dynamics of proton in the hydrogen bonds system. It should be emphasized that the long component of the $T_1$ ($^1$H) reveals quite complex temperature behaviour over the high temperature range covering all the PTs (see Fig. 11). The (IV→III) and (III→II) PTs are accompanied by the step wise changes in the $T_1$ value but its magnitude in phase III is lower than that in phases IV and II. The highest temperature PT is also accompanied by a sudden decrease of the $T_1$ value which remains, however, constant over the phase I (within the experimental error). Above 421 K only one component of proton relaxation time $T_1$ has been detected (27 ms). In this temperature region the free induction decay (FID) function becomes definitely elongated, what corresponds to the liquid-like behaviour of the relaxing protons.

Before reaching the phase transition (IV→III), above 344 K, the short component of the proton $T_1$ (of about 0.5 ms) appears and exists over the phase III with the constant value. This component is also present in phase II but with the time $T_1$ longer of about two orders than in the phase III. The short component was also detected in the low temperatures region, between 83 and 100 K.

The temperature dependence of the $^{19}$F spin–lattice $T_1$ relaxation time shows, analogically to the $^1$H $T_1$, wide, slightly asymmetric minimum, but with values ten times shorter. Similarly as in the case of the proton $T_1$ data, the fluorine $T_1$ at low temperatures is characterized by two weekly shaped minima of comparable depth – 18 and 20 ms – at about 130 K and 185 K, respectively. Below 135 K the long component of $^{19}$F spin–lattice relaxation time exists and its values are comparable to the proton $T_1$. Similar magnitudes of both relaxation times may suggest that the $^{19}$F nuclei of anion effectively relax to the lattice by the random modulations of the H–F dipole–dipole interactions due to the reorientation of the cation. Above 135 K only one exponential recovery function shape is found. It should be underlined that the change from the regular increasing to the decreasing of $^{19}$F spin–lattice relaxation times occurs at c.a. 364 K and coincides with the (IV→III) PT temperature. The fluorine spin–lattice relaxation time is insensitive to the (III→II) PT but experiences a rapid drop at the (II→I) PT reaching a constant value of $T_1$.

The $^1$H and $^{19}$F $T_1$ data between 83 K and the maximum on the $T_1$ (T) curve (316 K for protons, 364 K for fluorine nuclei) reflect the reorientation of moieties of the $[NH_2(CH_2)_4NH][BF_4]$ compound. The differences of the slopes of both arms of the analyzed minimum and a relatively wide temperature range, where the minimum values are constant, suggest that there are two nonequivalent cations in the phase IV.

Our preliminary interpretation of NMR results is restricted to the discussion of the energy activation. The experimental points

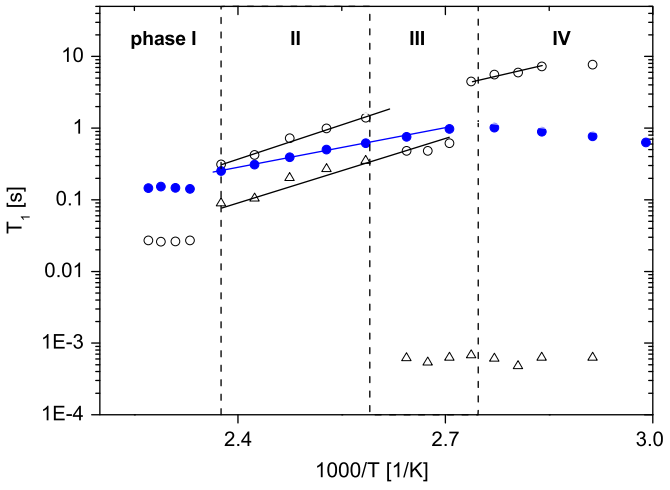


**Fig. 11.** Spin–lattice relaxation time, $T_1$, versus reciprocal temperature in the vicinity of phase transitions.

may be fit by the standard BPP equation:

$$\frac{1}{T_1} = \sum_{i=1}^{3} C_i \left[ \frac{\tau_{ci}}{1+\omega^2\tau_{ci}^2} + \frac{4\tau_{ci}}{1+4\omega^2\tau_{ci}^2} \right] \quad (1)$$

with $\tau_{ci}$ as the correlation time of the motion involved in the relaxation process according to the Arrhenius law ($\tau_c = \tau_0 \exp(E_a/RT)$, where $\tau_0$ is the correlation time at the limit infinite temperature), $E_a$ is the height of the barrier, $R$ – gas constant), $\omega$ – the Larmor angular frequency, and $C_i$ – the dipolar relaxation constant.

In the low temperature region ($T < 300$ K) the estimated $E_a$ values of the proton spin–lattice relaxation time are: 10.5 kJ/mol and 14.6 kJ/mol for the left and the right side of $T_1$ minimum, respectively. The reorientation of the piperazinium(+) cations which form strong organic chains is rather excluded below room temperature. On the other hand the estimated value of $E_a$ are similar to those found for numerous ionic salts containing piridinium cation for which the dynamics of protons of the NH group governs the relaxation mechanism [23–25]. In our opinion the $T_1$ temperature behaviour at low temperatures in $[NH_2(CH_2)_4NH][BF_4]$ may be explained in terms of the dynamics of protons engaged in the N−H···N hydrogen bonds. This motion is coupled with the reorientations of the $[BF_4]^-$ groups. For the $^{19}F$ spin–lattice relaxation time the corresponding $E_a$ values are 13.9 kJ/mol and 17.8 kJ/mol. Such magnitudes of activation energies suggest that at the beginning, at low temperatures, $[BF_4]^-$ anions perform anisotropic reorientation about three- or two-fold axis and subsequently, when temperature is increasing, the fast isotropic reorientation of $[BF_4]^-$ anions occurs [26,27]. In turn, the found maxima on both $T_1$ (T) curves ($^1H$ and $^{19}F$) at high temperatures, separated by nearly 50°, demonstrate the beginning of domination of translational effects over the reorientational motion. The analysis of the slopes of linear part of $T_1$ versus temperature curve above the maximum gives distinctly higher $E_a$ values: 64 kJ/mol for proton $T_1$ data (phase II), 38.6 kJ/mol (phase IV) and 34.7 kJ/mol for $^{19}F$ $T_1$ data (phase II and III). Relatively high values of estimated $E_a$ can provide the explanation of observed molecular dynamics as molecular translation diffusion through the lattice or proton conductivity.

## 9. IR studies

The infrared (in nujol and KBr) as well as Raman spectra of $[NH_2(CH_2)_4NH][BF_4]$ are presented in Fig. 14 in Supplementary materials whereas the tentative assignments of the bands are presented in Table 3. The assignments proposed in Refs. [28–33] were used as guides.

Fig. 12 shows the temperature evolution of the IR spectra in the region where the $[BF_4]^-$ bending mode at 534 $cm^{-1}$ is found. This band is not, however, significantly affected by the phase transitions what may indicate that the phase transitions do not influence strongly dynamics of the $[BF_4^+]$ cations. However, on the other hand, much more spectacular changes in the spectra are observed in the wavenumber range 625–575 $cm^{-1}$, i.e. region where the vibrations assigned to $[BF_4]^-$ as. stretch, (NH) deform. and $(CH_2)$ deform. modes are observed. The most important change is observed for the band at 605 $cm^{-1}$ which does not change position in phase IV but its frequency shifts towards lower values of about 5 $cm^{-1}$ in phase III. Moreover the absorbance of this band lowers with increasing of the temperature and the biggest drop takes place in phase III. It is worth of note that in phase III two extra bands of low intensity appear (at about 610 and 620 $cm^{-1}$) and they do not exhibit significant changes at III↔II PT temperature. Figs. 15 and 16 which show the temperature evolution of the IR spectra in the wavenumbers range 1700–1475 $cm^{-1}$ and 3400–3050 $cm^{-1}$, respectively, are included in Supplementary materials.

**Table 3**
Wavenumbers ($cm^{-1}$), in Nujol and in Fluorolube* medium, relative intensities and tentative assignments of the bands observed in the infrared and Raman spectra at room temperature.

| Band | | Assignment |
|---|---|---|
| IR | Raman | |
| 3324s, 3324*vs, 3313s, | 3323m | $(NH_2)^+$ as. stretch., (NH) stretch. |
| 3225s, 3223*vs | 3221vw | |
| 3175w | | (NH) Fermi resonance |
| | 3027m | |
| 2995*m | 2992vs | |
| 2956*w | | |
| 2877*m | 2878m | |
| 2776sh, 2715sh, 2618w, 2614*w | | |
| 2584sh | | |
| 2415m, 2414*m | | (NH) stretch. |
| 2212w, 2096vw, 1936sh,1802sh | | |
| 1631m, 1632*m | | $(NH_2)^+$ deform. |
| 1623sh | | |
| 1573w | | (NH) deform. |
| 1505*m,1503w | | (C–C) stretch |
| 1466*vs,1464vs | | $(CH_2)$ as. deform. |
| | 1456s | |
| 1445*s | 1444m | $(CH_2)$ sciss. |
| 1419m, 1419*m | | |
| 1374m, 1372*s | | $(CH_2)$ as. deform. |
| 1326m, 1326*s | | (CNH) deform. |
| | 1317s | |
| 1310m, 1309*m | | (CCH) deform. |
| 1293w,1247w | | |
| 1202m | | |
| 1177m | 1180w | $[BF_4]^-$ stretch., (CH) deform. |
| 1082ss | 1066m | $[BF_4]^-$ stretch, (CH) sciss. |
| 1062vs | | $[BF_4]^-$ as. stretch, (CH) out of plane |
| | 1046m | Ring deform. |
| 1029vs | 1018m | $[BF_4]^-$ stretch |
| 973s | | (CH) bending |
| 876vw,863m | | |
| 850s | | |
| | 839w | |
| 817s | 820vs | $[BF_4]^-$ as. stretch |
| 809w | | (NH) deform. |
| 767w | 768s | $(CH_2)$ deform. |
| 723vw | | |
| 605m,599w | | |
| 589sh | | |
| 534sh | | $[BF_4]^-$ bending |
| 526w | | |
| 522m | 522m | |
| 517m | | |
| 458w | 478m,465m | |
| | 425m | |
| 348s | | $[BF_4]^-$ bending |
| 310m | | |
| 232,157 | | Lattice modes |

vs – very strong; s – strong; m – medium, w – weak; vw – very weak; sh – shoulder.

## 10. Discussion

$[NH_2(CH_2)_4NH][BF_4]$ was found to undergo a complex sequence of structural phase transitions (PTs):

| Phase | IV | III | II | I |
|---|---|---|---|---|
| $T_c/K(\Delta S/J\ mol^{-1}\ K^{-1})$ | 364(7.6) | 386(6.5) | 421 | (11.2) |

where $T_c$ is given for the heating cycle.

The molecular mechanism of PTs has been studied by several experimental techniques: X-ray diffraction, thermal methods as well

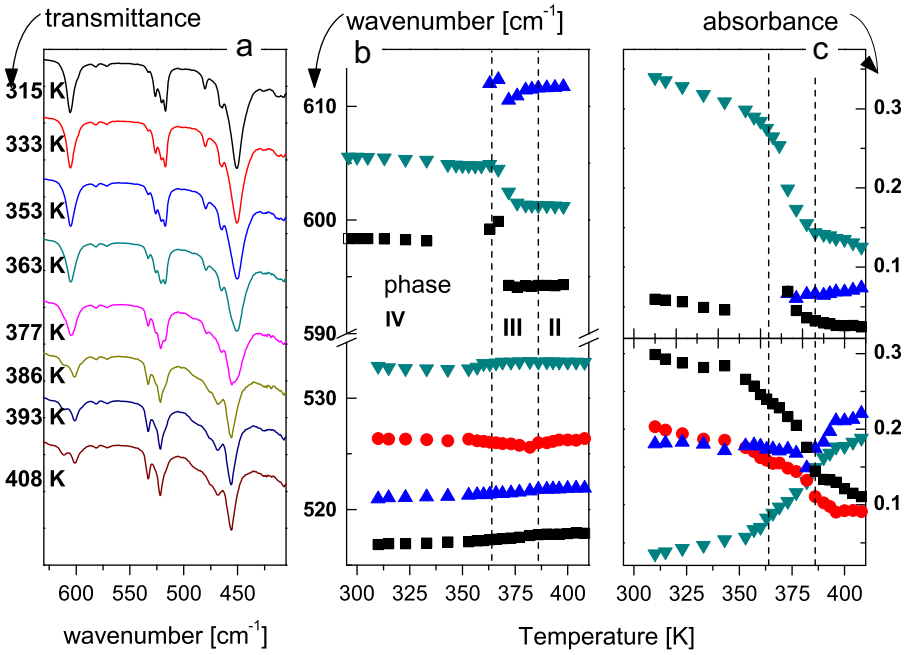


**Fig. 12.** (a) Temperature evolution of the FT-IR spectra in the frequency region assigned to the $[BF_4]^-$ bending, $[BF_4]^-$ as. stretch, (NH) deform. and $(CH_2)$ deform. bands, (b) temperature dependence of the wavenumbers and (c) temperature dependence of the absorbance of the bands of $[NH_2(CH_2)_4NH][BF_4]$ crystal in the region 625–400 $cm^{-1}$.

as the dielectric, NMR ($^1H$ and $^{19}F$) and vibrational (IR) spectroscopy. From the point of view of thermodynamic properties (DSC) detected PTs are characterized by an "order-disorder" mechanism. The estimated total entropy transition ($\Delta S_1+\Delta S_2+\Delta S_3 \approx 25$ J/mol K) suggests that the highest temperature phase I is distinguished by a high disorder of the cationic and anionic sublattices. The $^1H$ and $^{19}F$ spin–lattice relaxation measurements allows us to separate to a certain extent the contribution of individual sublattices to the successive PTs. The IV→III PT is clearly active in the $^1H$ whereas weakly in the $^{19}F$ $T_1$ measurements. It means that the transition entropy effect ($\Delta S_1 = 7.6$ J/mol K) may be explained by a change in dynamics of the hydrogen bonds system (N−H···N and N−H···F) and onset of the reorientational motion of the $[BF_4]^-$ moieties. Subsequently, the III→II PT is inactive in the $^{19}F$ $T_1$ relaxation thus the anionic sublattice is not expected to contribute to this PT mechanism. The entropy effect $\Delta S_2$ may be due to the motion of the piperazinium(+) cations and the change in the hydrogen bonds system. In turn, the II→I PT is strongly active in the $^1H$ and the $^{19}F$ $T_1$ relaxation thus both anionic and cationic sublattices are involved in the transition mechanism. We can postulate that $[BF_4]^-$ and $[NH_2(CH_2)_4NH]^+$ moieties in the phase I are either able to perform the overall motion or translation diffusion and the proton conductivity contributes to the phase transition as well.

The IV→III and II→I PTs are accompanied by a significant change in the electric polarization of the system. The dielectric increment values are comparable for both transitions, being of the order of 15–50 units (from 2 MHz to 4.2 kHz). These dielectric anomalies may be explained in terms of the motion of dipolar groups. The symmetric tetrahedral $[BF_4]^-$ units are not bestowed an essential dipole moment thus dynamics of the anionic moieties does not contribute to the dielectric increment/polarization. In order to explain the origin of the dielectric anomalies at 364 and 421 K we have to consider two possibilities: (i) reorientational motion of strongly dipolar piperazinium(+) cations (permanent dipole moment), (ii) proton motion which leads to the change in the resultant dipole moment of hydrogen bonds system/unit cell. For the lowest temperature IV→III PT the second possibility (ii) is more probable. The onset of motion of the piperazinium(+) cations takes place undoubtedly at the II→III (probably a small-angle libration) which is accompanied by a minor dielectric anomaly. The mechanism of molecular motions in the vicinity of the II→I PT seems to be rather complicated because we should take into account the following motions: the overall reorientation or self-diffusion of both the piperazinium(+) and $[BF_4]^-$ units as well as the proton conductivity. An additional information about the molecular mechanism of PTs results also from the electric conductivity measurements. The conductivity contributes to the dielectric loss in the vicinity of the IV→III and II→I PTs. The significant increase of the conductivity especially just before the 421 K indicates clearly the beginning of the collective processes implied as a motion of protons or $[BF_4]^-$ units. Over the phase I the activation energy equals to 1 eV (see Fig. 7) and the characteristic of the conductivity versus $1/T$ confirms the proton and the $[BF_4]^-$ anions motions. The interpretation of the dielectric results is consistent with our $^1H$ and $^{19}F$ NMR $T_1$ data.

The infrared studies showed that the vibrational states of the piperazinium(+) cations and tetrafluoroborate anions change markedly through the structural PTs at 364 and 386 K. The most sensitive to the PT appeared to be the 605 $cm^{-1}$, 598 ($[BF_4]^-$ as. stretch., (NH) deform., $(CH_2)$ deform.), 1630($(NH_2)^+$ deform.), 1505 (C–C stretching), 3324, 3313, 3225 ($(NH_2)^+$ as. stretch., (NH) stretch.) modes. Quite surprising is the fact that the intensity of the peaks is more sensitive on the PTs than the position of the peaks. The increase of the half width of the majority of bands is related to the subsequent release of the motion of the moieties what is also confirmed by NMR and dielectric results.

It is interesting to refer to the ferroelectrics based on organic 1,4-diazobicyclo[2,2,2]octane (abbreviated dabco) [34–36]. This group consists of three crystals of a general formula $[C_6H_{13}N_2]^+X^-$ where $X$ stands for the tetrahedral anions: $[ClO_4]^-$, $[BF_4]^-$ and $[ReO_4]^-$. It was shown that one-dimensional $NH^+\cdots N$ bonded aggregates are essential for the ferroelectric order. In the case of $dabcoBF_4$ and $dabcoClO_4$ the proton motion in the $NH^+\cdots N$ bonds was coupled to the dynamical disordering of the anions. It should be emphasized that $N\cdots N$ distance in the homoconjugated polycations of $dabcoBF_4$ and $dabcoClO_4$ is 2.841(5) and 2.839(7) Å, respectively, at 293 K, whereas in $[NH_2(CH_2)_4NH][BF_4]$ the N2···N3 equals to 2.87(1) Å and

N4···N1 to 2.86(1) Å. From the point of view of the N–H···N hydrogen bonds system the compared compounds reveal large similarities. Thus the molecular mechanism of the IV→III PT in $[NH_2(CH_2)_4NH][BF_4]$ seems to have the same origin as in dabco analogues.

It must be emphasized that the titled compound represents the first organic–inorganic simple salt containing the single-protonated piperazinium cation which was studied by means of the wide variety of experimental techniques. A survey of Cambridge Structural Database (CSD version 5.32 (November 2010) & updates (May 2011)) shows that among all structures consisting of the piperazinium(+) and (2+) cations only ca. 5% contain monocations. Among these structures only one hybrid organic–inorganic material (piperazinium nitrate characterized structurally [22]) was found.

### 10.1. Conclusions

1. $[NH_2(CH_2)_4NH][BF_4]$ (PBF) contains a single protonated piperazinium cations which were found to form in the crystal structure strong linear N–H···N hydrogen bonded chains (extremely rare in the ionic piperazinium compounds).
2. PBF was found to undergo three high temperature structural phase transitions governed by the $[BF_4]^-/[NH_2(CH_2)_4NH]^+$ ions and protons motion.
3. The highest temperature phase revealed the features characteristic of either the self-diffusion of ions or proton conductivity.
4. The title $[NH_2(CH_2)_4NH][BF_4]$ crystal is piezoelectric and polar at room temperature what makes it potentially applicable in NLO devices. The properties result from the unique structure where all the bistable $NH^+\cdots N$ hydrogen bonds are parallel and directed exactly in the same sense. The dynamic of proton and $[BF_4]^-$ groups is responsible for the temperature dependent changes of the material and stabilization of the subsequent phases.

## Appendix A. Supplementary material

Fig. 13 presents the dilatometric measurements results. Scans were carried out perpendicular to the biggest plate of the sample what was the $[20\bar{1}]$ direction. All the phase transitions are manifested by the increase of the $\Delta L/L_0$ value on heating.

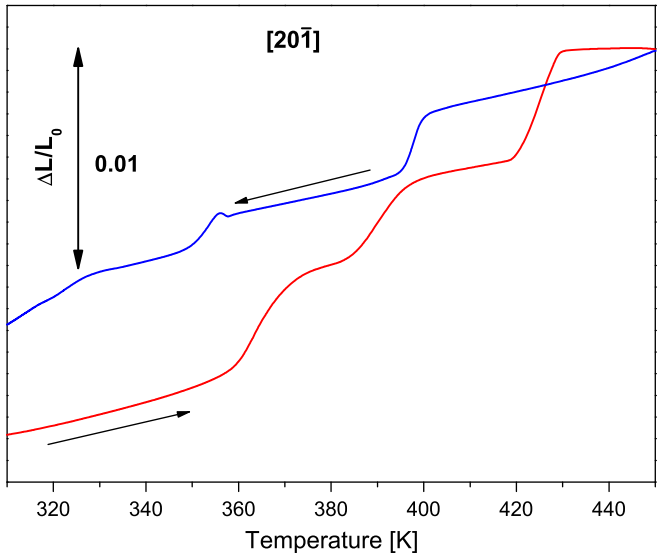


**Fig. 13.** Change of dimensions of the $[NH_2(CH_2)_4NH][BF_4]$ recorded in the $[20\bar{1}]$ direction.

**Table 4**
Selected geometric parameters (Å) at 295 K.

| | | | |
|---|---|---|---|
| **Piperazinium A** | | **Piperazinium B** | |
| N1–C1 | 1.466 (4) | N3–C6 | 1.443 (5) |
| N1–C2 | 1.478 (5) | N3–C7 | 1.468 (5) |
| N2–C3 | 1.473 (5) | N4–C8 | 1.478 (5) |
| N2–C4 | 1.463 (5) | N4–C5 | 1.492 (5) |
| C2–C4 | 1.494 (5) | C5–C7 | 1.501 (5) |
| C1–C3 | 1.522 (6) | C6–C8 | 1.491 (5) |
| $[BF_4]^-$(**I**) | | $[BF_4]^-$(**II**) | |
| B1–F1 | 1.382 (5) | B2–F6 | 1.365 (5) |
| B1–F2 | 1.338 (5) | B2–F5 | 1.286 (5) |
| B1–F3 | 1.333 (5) | B2–F8 | 1.363 (5) |
| B1–F4 | 1.333 (5) | B2–F7 | 1.385 (5) |

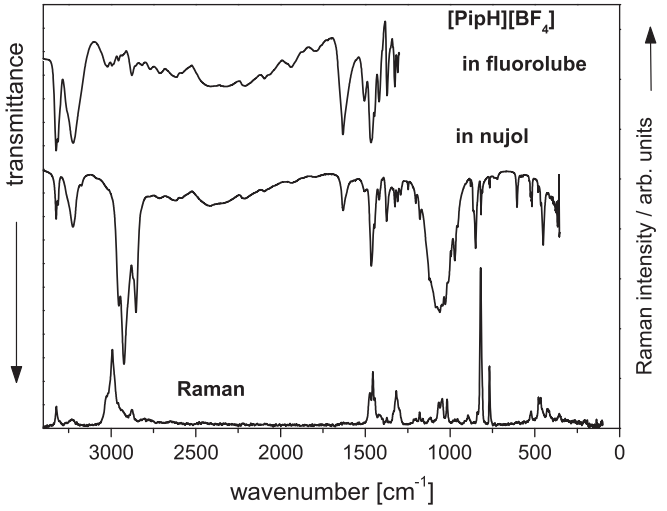


**Fig. 14.** Infrared (in fluorolube and nujol) and Raman powder spectra of $[NH_2(CH_2)_4NH][BF_4]$ at ambient temperature.

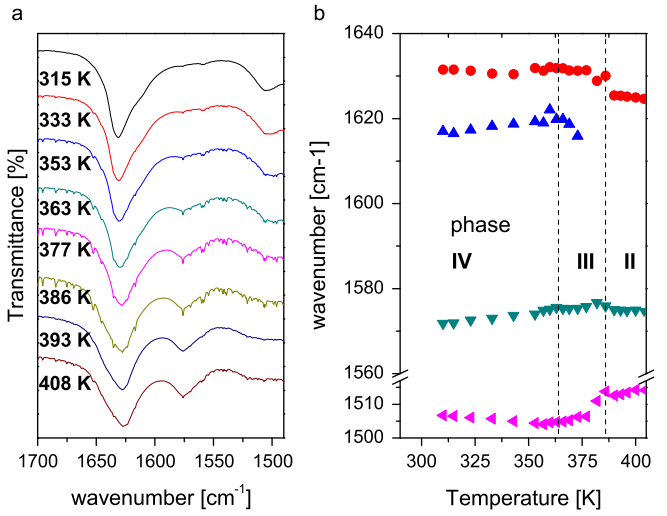


**Fig. 15.** (a) Temperature evolution of the FT-IR spectra in the frequency region assigned to the $(NH_2)^+$ deformation, (NH) deformation and (C–C) stretching bands and (b) temperature dependence of the wavenumbers of $[NH_2(CH_2)_4NH][BF_4]$ crystal in the region 1700–1475 $cm^{-1}$.

Although in the III→II PT the crystal sample become opaque all PTs are well reproducible.

Table 4 presents the selected geometric parameters of $[NH_2(CH_2)_4NH][BF_4]$ at 295 K.

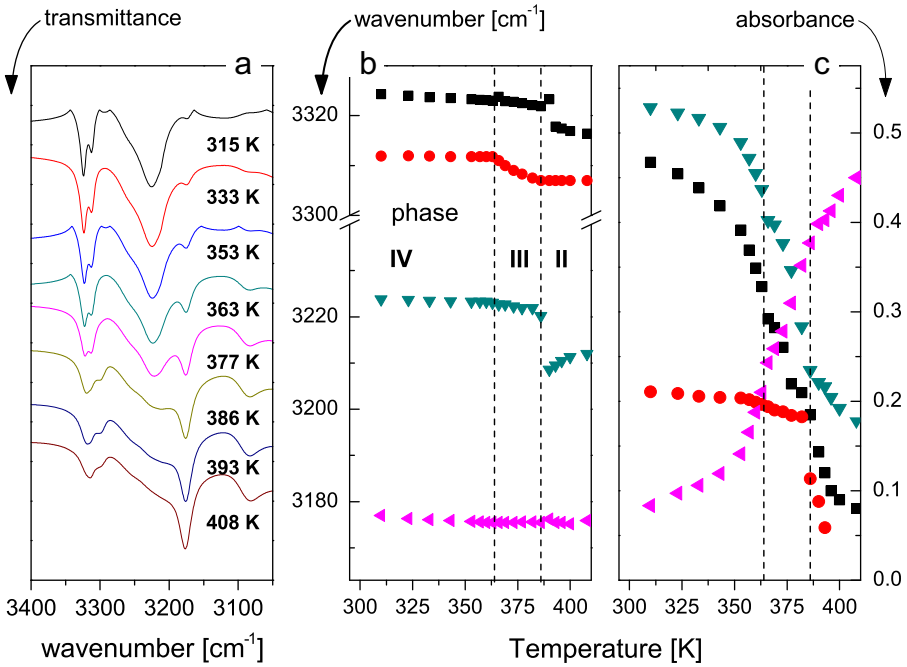


**Fig. 16.** (a) Temperature evolution of the FT-IR spectra in the frequency region assigned to the $(NH_2)^+$ stretching and (NH) stretching bands, (b) temperature dependence of the wavenumbers and (c) temperature dependence of the absorbance of $[NH_2(CH_2)_4NH][BF_4]$ crystal in the region 3400–3050 $cm^{-1}$.

The infrared (in nujol and KBr) as well as Raman spectra of $[NH_2(CH_2)_4NH][BF_4]$ are presented in Fig. 14.

Fig. 15 presents the IR spectra of $[NH_2(CH_2)_4NH][BF_4]$ in the region 1700–1475 $cm^{-1}$. In this wavenumber range the vibration of piperazinium(+), both ring and amino group, are manifested in spectrum. The successive phase transitions in $[NH_2(CH_2)_4NH][BF_4]$ is reflected in the spectrum. Namely: the band at 1630 $cm^{-1}$ softens in phase III and drops at III↔II PT temperature, the shoulder component of peak at about 1623 $cm^{-1}$ hardens in phase IV and then softens in phase III until it fades before III↔II PT; the peak at 1573 $cm^{-1}$ appears at phase III where it hardens and starts to soften in phase II; the peak at 1503 $cm^{-1}$ decrease its frequency approaching IV↔III PT temperature and then hardens in phases III and II, with tiny discontinuity at III↔II PT.

The region of 3400–3050 $cm^{-1}$ is shown in Fig. 16. Two peaks at around 3320 $cm^{-1}$ shift towards lower wavenumbers. The position of the band at 3324 $cm^{-1}$ is clearly influenced by the III→II whereas the position of the band at 3313 $cm^{-1}$ softens in phase III and in phase II does not change its position. The band at about 3220 $cm^{-1}$ drop of about 10 $cm^{-1}$ at III→II PT and then hardens in phase II. One may note that only the 3180 $cm^{-1}$ band's intensity accrues whereas intensity of other bands drops. Similar to the region of 600 $cm^{-1}$ the biggest decrease is visible in phase III.

## Appendix B. Supplementary data

Supplementary data associated with this article can be found in the online version at doi:10.1016/j.jssc.2011.12.020.

## References

[1] G.R. Desiraju, Nature 412 (2001) 397.
[2] S. Horiuchi, Y. Tokura, Nat. Mater. 7 (2008) 357.
[3] J.-L. Lehn, Supramolecular Chemistry: Concepts and Perspectives, VCH Publishers, New York, 1995.
[4] J. Zyss, Molecular Nonlinear Optics: Materials, Physics and Devices, Academic Press, New York, 1993.
[5] F. Agullo-Lopez, J.M. Cabrera, F. Agullo-Rueda, Electrooptics: Phenomena, Materials and Applications, Academic Press, New York, 1994.
[6] G.H. Haertling, J. Am. Ceram. Soc. 82 (1999) 797.
[7] N.J. Long, Angew. Chem. Int. Ed. 34 (1995) 21.
[8] G. Xu, G.-G. Guo, M.-S. Wang, Z.-J. Zhang, W.-T. Chen, J.-S. Huang, Angew. Chem. Int. Ed. 46 (2007) 3249.
[9] Q. Ye, D.-W. Fu, H. Tian, R.-G. Xiong, P.W.H. Chan, S.D. Huang, Inorg. Chem. 47 (3) (2008) 772–774.
[10] D.-W. Fu, W. Zhang, R.-G. Xiong, Cryst. Growth Des. 8 (9) (2008) 3461–3464.
[11] P. Czarnecki, W. Nawrocik, Z. Pająk, J. Wąsicki, J. Phys.: Condens. Matter 6 (1994) 4955.
[12] P. Czarnecki, W. Nawrocik, Z. Pająk, J. Wąsicki, Phys. Rev. B 49 (1994) 1511.
[13] J. Wąsicki, P. Czarnecki, Z. Pająk, W. Nawrocik, W. Szczepański, J. Chem. Phys. 107 (1997) 576.
[14] Z. Pająk, P. Czarnecki, J. Wąsicki, W. Nawrocik, J. Chem. Phys. 109 (1998) 6420.
[15] Z. Pająk, H. Małuszyńska, B. Szafrańska, P. Czarnecki, J. Chem. Phys. 117 (2002) 5303.
[16] Z. Pająk, P. Czarnecki, B. Szafrańska, H. Małuszyńska, Z. Fojud, J. Chem. Phys. 124 (2006) 144502.
[17] Z. Pająk, P. Czarnecki, B. Szafrańska, H. Małuszyńska, Z. Fojud, Phys. Rev. B 69 (2004) 132102–132104.
[18] M. Wojtaś, A. Gągor, O. Czupiński, A. Pietraszko, R. Jakubas, J. Solid State Chem. 182 (2009) 3021.
[19] M. Wojtaś, A. Gągor, O. Czupiński, A. Bil, Z. Tylczyński, D. Isakov, A. Pietraszko, R. Jakubas, Phys. Rev. B 83 (2011) 144103.
[20] Oxford Diffraction (2007). CrysAlis CCD and CrysAlis RED (including SCALE3 ABSPACK). Oxford Diffraction Ltd, Abingdon, England.
[21] G.M. Sheldrick, Acta Crystallogr. A 64 (2008) 112–122.
[22] G. Perpetuo, J. Janczak, Acta Crystallogr. E 61 (2005) o2531.
[23] W. Medycki, R. Jakubas, Solid State Nucl. Magn. Reson. 21 (2002) 44.
[24] J. Jóźków, W. Medycki, J. Zaleski, R. Jakubas, G. Bator, Z. Ciunik, Phys. Chem. Chem. Phys. 3 (2001) 3222.
[25] J. Tarasiewicz, R. Jakubas, G. Bator, J. Zaleski, J. Baran, W. Medycki, J. Mol. Struct. 932 (2009) 6.
[26] H. Ono, R. Seki, R. Ikeda, H. Ishida, J. Mol. Struct. 345 (1995) 235.
[27] E. Mikuli, B. Grad, W. Medycki, K. Hoderna-Natkaniec, J. Solid State Chem. 177 (2004) 3795.
[28] D. Havlicek, V. Chudoba, I. Nemec, I. Cisarova, Z. Micka, J. Mol. Struct. 606 (2002) 101.
[29] O. Czupiński, R. Jakubas, A. Pietraszko, J. Mol. Struct. 704 (2004) 177–187.
[30] B. Quin, J. Lin, Z. Lin, H. Ren, Y. Xue, Spectrochim. Acta Part A 61 (2005) 717.
[31] N.E. Heime, R.E.D. Sesto, Z. Meng, J.S. Wilkes, W.R. Carper, J. Mol. Liq. 124 (2006) 84.
[32] A.M. Petrosyan, Vib. Spectros. 43 (2007) 284.
[33] M.K. Marchewka, A. Pietraszko, Spectrochim. Acta Part A 69 (2008) 312.
[34] A. Katrusiak, M. Szafrański, Phys. Rev. Lett. 82 (1999) 576.
[35] A. Budzianowski, A. Katrusiak, M. Szafrański, J. Phys. Chem. B 112 (2008) 16619.
[36] M. Szafrański, A. Katrusiak, G. McIntyre, Phys. Rev. Lett. 89 (2002). 215507-1-4.